Tornado Frequency in the United States Related to Global Relative Angular Momentum

VITTORIO A. GENSINI

Meteorology Program, College of DuPage, Glen Ellyn, Illinois

ALAN MARINARO

Meteorology Program, Northern Illinois University, DeKalb, Illinois

(Manuscript received 21 August 2015, in final form 4 November 2015)

ABSTRACT

Global relative angular momentum and the first time derivative are used to explain nearly an order of magnitude of the variability in 1994–2013 U.S. boreal spring tornado occurrence. When plotted in a phase space, the global wind oscillation (GWO) is obtained. This global index accounts for changes in the global budget of angular momentum through interactions of tropical convection anomalies and extratropical dynamics including the engagement of surface torques. It is shown herein that tornadoes are more likely to occur in low angular momentum base states and less likely to occur in high angular momentum base states. When excluding weak GWO days, a maximum average of 3.9 (E)F1+ tornadoes per day were found during phase 1. This decreases to a minimum of 0.9 (E)F1+ tornadoes per day during phase 5. Composite environmental analysis suggests that increases/decreases in tornado occurrence are closely associated with anomalies in tropospheric ingredients necessary for tornadic storms. In addition, tornado frequency days exceeding the 90th percentile are shown to be favored when the global relative angular momentum budget and first time derivative are negative (GWO phases 1 and 2), as are significant tornado events [(E)F2+]. Implications for using GWO as a predictor for tornado forecasting are also discussed.

1. Introduction

On the morning of 25 March 1948, the first modern tornado forecast was disseminated at Tinker Air Force Base in Oklahoma City, Oklahoma, by Major E. J. Fawbush and Captain R. C. Miller (Grice et al. 1999). Fawbush and Miller's successful forecast of a tornado near the Air Force base that afternoon proved to be a turning point in modern-day severe weather forecasting. Today, nearly seven decades later, official severe weather forecasts in the United States originate from the Storm Prediction Center in Norman, Oklahoma, and are issued as many as eight days in advance. Substantial research progress over this period has led to better understanding of the atmospheric ingredients (Doswell et al. 1996) necessary for tornado formation. For example, it is well known that low static stability, high surface water vapor mixing ratios, and adequate shear in the vertical profile of wind leads to favorable conditions for the development of supercell thunderstorms capable of spawning tornadoes.

Owing to the relatively small space ($\sim 10^{-1}$ km) and time ($\sim 10^{3}$ s) scales of tornadoes, their prediction remains a challenging task. This is especially true of tornado occurrence in the subseasonal-to-seasonal time scales, which is beyond the extent of most medium range (up to two weeks) numerical weather prediction solutions. This two-week to two-month forecast period is a novel area of research in regards to extreme weather events. In fact, the World Meteorological Organization (WMO) published a research implementation plan in 2010 to enhance forecasts at these time scales, which has now grown into the Subseasonal-to-Seasonal Prediction Project (S2SPP; Brunet et al. 2010). Despite projects such as S2SPP, subseasonal prediction of U.S. severe weather is in its infancy. Recent research has focused mainly on jet stream configurations associated with phases of El Niño–Southern Oscillation (ENSO; Cook and Schaefer 2008; Allen et al. 2015) and upstream Rossby wave dispersion from longitudinal placement of

Corresponding author address: Vittorio A. Gensini, Meteorology Program, College of DuPage, 425 Fawell Blvd., Glen Ellyn, IL 60137.
E-mail: gensiniv@cod.edu

DOI: 10.1175/MWR-D-15-0289.1

anomalous equatorial convection associated with different Madden–Julian oscillation (MJO) phases (Barrett and Gensini 2013; Thompson and Roundy 2013; Barrett and Henley 2015). While these results have made a significant contribution to our understanding of subseasonal U.S. severe weather variability, they lack predictive skill when the dominant mode of Northern Hemisphere tropospheric variability is not driven through tropical convection and its associated meridional dispersion of Rossby waves. Thus, this research utilizes atmospheric angular momentum (AAM) to account for additional extratropical forcing mechanisms on downstream Rossby wave dispersion (Oort 1997).

AAM provides a convenient diagnostic metric in which to track subseasonal changes in Rossby waves and their associated regional impacts on sensible weather (Langley et al. 1981; Peixoto and Oort 1992). Convective anomalies associated with the MJO were first thought to have the greatest contributions on AAM (Anderson and Rosen 1983; Madden 1987). However, further research in the 1990s proposed approximately equal roles for friction and mountain torque in forcing global relative AAM budget changes (Weickmann et al. 1992; Madden and Speth 1995; Hendon 1995; Weickmann et al. 1997). The forcing terms influencing global AAM were brought together using a global synoptic–dynamic model (GSDM; Weickmann and Berry 2007), whose application to real-time forecasting requires monitoring of global relative AAM (M_R) and its time tendency (dM_R/dt). This real-time monitoring of M_R and dM_R/dt was first described as the global wind oscillation (GWO) by Weickmann and Berry (2009). The GWO is broadly defined by eight phases (1, 2, 3, 4, 5, 6, 7, and 8).

Given the recent success of using the MJO to explain modulation in U.S. tornado (Barrett and Gensini 2013; Thompson and Roundy 2013) and severe hail (Barrett and Henley 2015) frequency, the GWO should serve to increase our understanding of variability associated with these extreme events. The GWO encompasses the MJO and various other extratropical processes (e.g., meridional momentum transports, frictional torque, mountain torque) known to influence the global AAM budget. The relationship of GWO to severe weather in the United States was explored in a case study where specific GWO phases were identified and used to forecast a mid- and upper-tropospheric trough in the southwestern United States two weeks in advance, which resulted in hazardous convective weather (including tornadoes) during the period 20–23 May 2007 on the Great Plains of the United States (Weickmann and Berry 2009). Given this evidence, and the known influence of the MJO, this study focuses on analyzing the frequency of U.S. tornadoes (and their associated environments) by phase of the GWO.

2. Data and methods

Tornado data were retrieved from the Storm Prediction Center's online database (NOAA/NWS Storm Prediction Center 2015] for March–June during the period 1994–2013. Classifications of tornado days were sorted into one of eight GWO phases following the Earth System Research Laboratory's (ESRL) GWO product daily dataset (available online at http://www.esrl.noaa.gov/psd/map/clim/gwo.data.txt). GWO phase was determined using global relative M_R (GWO1) and dM_R/dt (GWO2) anomalies utilizing a phase space diagram first created for the MJO (Wheeler and Hendon 2004). Daily GWO1/GWO2 standardized anomalies are given in the ESRL dataset alongside GSDM stage, as well as GWO phase and amplitude. Following the methodology of Wheeler and Hendon (2004) for the MJO, the GWO was constructed by plotting dM_R/dt as a function of M_R itself. That was done so the variations of M_R would be similar in both phase spaces, allowing for a ''close match'' of the actual phases of the MJO and GWO (Weickmann and Berry 2009). As an example, the progression of GWO through phases 4, 5, and 6 can be thought of as increasing anomalies in the global M_R budget, whereas the progression through phases 8, 1, and 2 denotes decreasing anomalies (Weickmann and Berry 2009).

Data from the North American Regional Reanalysis (NARR; Mesinger et al. 2006) were used to create spatial anomalies of environmental parameters known to favor tornadic storms. Fields were downloaded online (NOAA/NCDC 2015) for each March–June day during 1994–2013, valid at 2100 UTC. The significant tornado parameter (STP; Thompson et al. 2003) calculation in this study closely resembles the fixed-layer calculation used in Thompson et al. (2003):

$$\mathrm{STP} = \frac{\mathrm{SBCAPE}}{1500} \times \frac{(2000 - \mathrm{SBLCL})}{1000} \times \frac{\mathrm{SRH01}}{150} \times \frac{\mathrm{BWD06}}{20},$$

using surface-based convective available potential energy (SBCAPE), surface-based lifting condensation level (SBLCL), 0–1-km storm relative helicity (SRH01), and 0–6-km bulk wind difference (BWD06). AGL height fields not contained in the NARR dataset were calculated by vertically interpolating NARR pressure fields to AGL height coordinates. In addition, STP was set to zero if surface-based convective inhibition was less than $-125\,\mathrm{J\,kg^{-1}}$.

Environmental standardized anomalies were calculated by subtracting March–June average values from average values in the valid GWO phase. A two-tailed Z

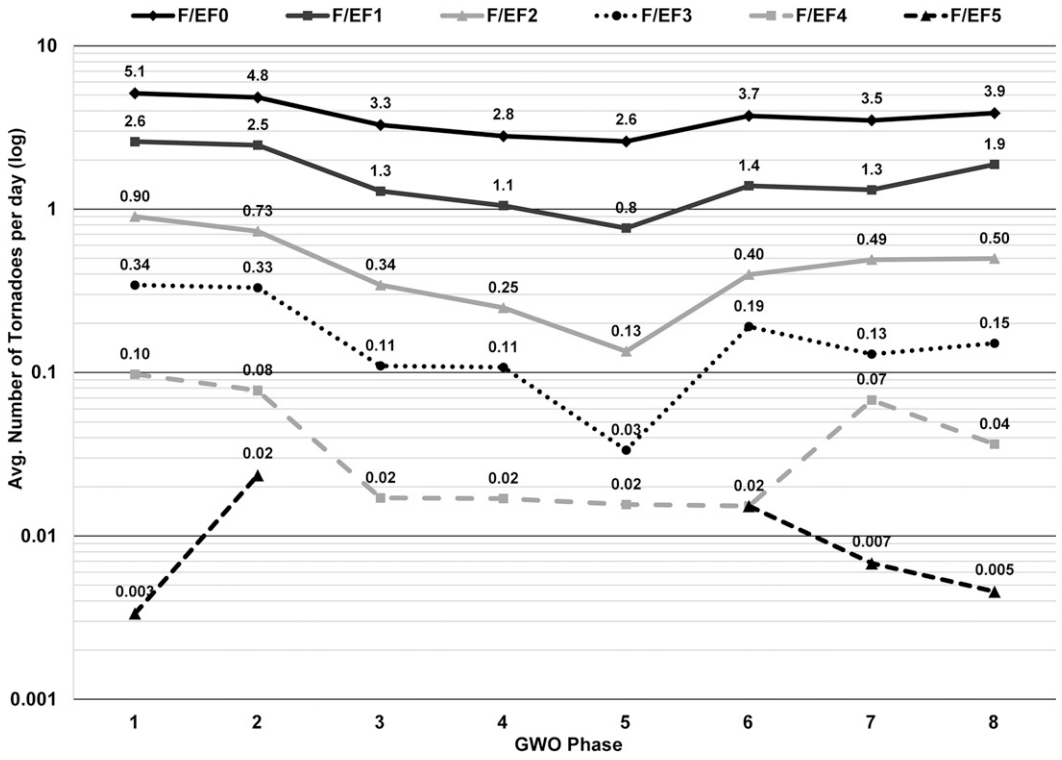

FIG. 1. March–June average number of tornadoes per day (log scale) by GWO stage during 1994–2013. As an example, an average of 5.1 (E)F0 tornadoes per day can be expected in GWO phase 1, decreasing to an average of 2.6 tornadoes per day in GWO phase 5.

test was conducted for statistical significance ($\alpha = 0.05$) for the average number of tornadoes per day and the raw count anomalies. Statistical significance ($\alpha = 0.05$) was calculated at each grid point for each GWO phase using a Mann–Whitney U test for the medians.

3. Results

a. Tornado frequency

Average U.S. tornado count per day is shown to vary by phase of the GWO. Over the 20-yr study (1994–2013), specific negative M_R (GWO phases 8, 1, and 2) regimes were most favorable for March–June U.S. tornado frequency, whereas positive M_R (GWO phases 4, 5, and 6) conditions were least favorable using various tornado occurrence metrics. These M_R half-stage clusters account for 62% and 19% of all (E)F1+ tornadoes, respectively. On average, a March–June day in GWO phase 1 was found to produce 8.6 tornadoes per day (Fig. 1). This value is roughly halved when analyzing GWO phase 5 (4.1 tornadoes per day). However, variability is best explained when the GWO amplitude is ≥1 (Weickmann et al. 1997). A total of 68.8% (1680) of March–June days were found to meet this criterion, tallying 4248 (E)F1+ tornadoes for an average of 2.5 (E)F1+ tornadoes per day. This increases to a maximum of 3.9 (E)F1+ tornadoes per day during GWO phase 1 and decreases to a minimum of 0.9 (E)F1+ tornadoes per day during phase 5. Other tornado strengths exhibit at least a doubling of average number of tornadoes per day from phase 1 to 5 (Fig. 1). When stratified by tornado strength, the range in the average number of tornadoes per day from GWO phases 1 to 5 accounts for nearly an order of magnitude change in the variability of U.S. springtime (E)F1+ tornadoes. Focusing only on the most violent tornadoes [i.e., those rated (E)F4 or (E)F5], GWO phases 1 and 2 account for 56% of these events. This increases to 65% when excluding weak GWO events. Interestingly, no (E)F5 tornadoes were recorded in phases 3, 4, or 5 during the study period. Cross-phase variability explained by the GWO is substantial, and has not been demonstrated to this magnitude by other known teleconnection indices [e.g., the North Atlantic Oscillation (NAO)]. A robust example is shown when analyzing (E)F1+ tornadoes during strong GWO events. During GWO phases 1 and 2, statistically significant positive tornado count and average tornado count per day anomalies are found. In contrast, phases 4 and 5 revealed negative counts and negative tornado count per day anomalies at the 95% confidence level (Fig. 2).

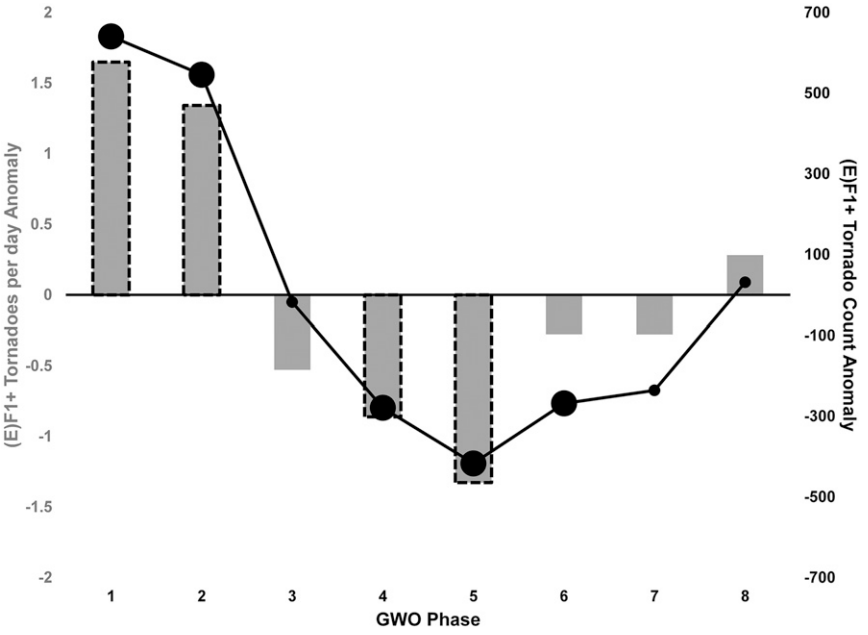

FIG. 2. Average March–June (E)F1 or greater tornadoes per day and the raw tornado count standardized anomalies by GWO phase during 1994–2013. The gray bars correspond to the left axis and the black line corresponds to the right axis. The dashed gray bars and large black dots denote statistical significance at the 95% confidence level.

b. Tornado environments

Variability in raw tornado counts and the average number of tornadoes per day is supported by conferring anomalies in tropospheric ingredients known to be present when tornadoes form. One of these ingredients, moisture, is typically diagnosed using dewpoint by forecasters. Using NARR, surface dewpoint tornado day standardized anomalies were created for each GWO phase against the background March–June climatological values valid at 2100 UTC each day. Phases 8, 1, and 2 exhibited positive surface dewpoint anomalies across a majority of the United States, whereas phases 5, 6, and 7 exhibited large spatial areas of negative surface dewpoint anomalies (Fig. 3). Positive and negative surface dewpoint anomalies are supported by the respective interphase 850-hPa geopotential height values. Positive surface dewpoint anomalies help contribute to an unstable atmosphere as measured by convective available potential energy (CAPE).

When combined with adequate vertical wind shear, this CAPE/shear parameter space can be used to diagnose significant severe weather potential from the environment (Brooks et al. 2003; Gensini and Ashley 2011). Here, the product of SBCAPE and BWD06 is used to examine the synoptic-scale favorability for such severe weather events (Fig. 4). It is common to see ridging in the western CONUS during GWO phases 4, 5, and 6 when SBCAPE anomalies are largely negative. This makes conceptual sense from a pattern recognition perspective, as midtropospheric northwesterly flow across the Great Plains would not favor poleward moisture flux from the Gulf of Mexico.

While CAPE/shear parameter space is a good indicator for the potential of organized severe weather, other factors are necessary for tornado producing thunderstorms. Thus, a more stringent environment was employed to diagnose vertical wind shear, instability, storm relative helicity, convective inhibition, and lifting condensation level (i.e., the STP). Large positive STP anomalies exist during GWO phase 1 in a region bounded by 30°–45°N and 85°–100°W (Fig. 5). Significant positive STP anomalies are strongly correlated with the spatial density of greatest tornado occurrence. Conversely, negative STP anomalies are strongly correlated with an absence of tornado occurrence during GWO phase 5. Other GWO phase STP anomalies explain the variability of tornado frequency quite admirably (Fig. 5). STP anomalies are linked to synoptic-scale meteorological conditions present during the time of tornadogenesis, such as those shown in Figs. 2 and 3. In essence, the transition through phases 8, 1, and 2 is associated with mountain and frictional torque trending negative (Weickmann and Berry 2009), which modulates a negative Pacific–North American (PNA; Mo and Livezey 1986) teleconnection pattern characteristic of mid- and upper-tropospheric troughing over the western United States (Weickmann 2003; Lott et al. 2001). The negative mode of the PNA is also correlated with the strength of the boreal

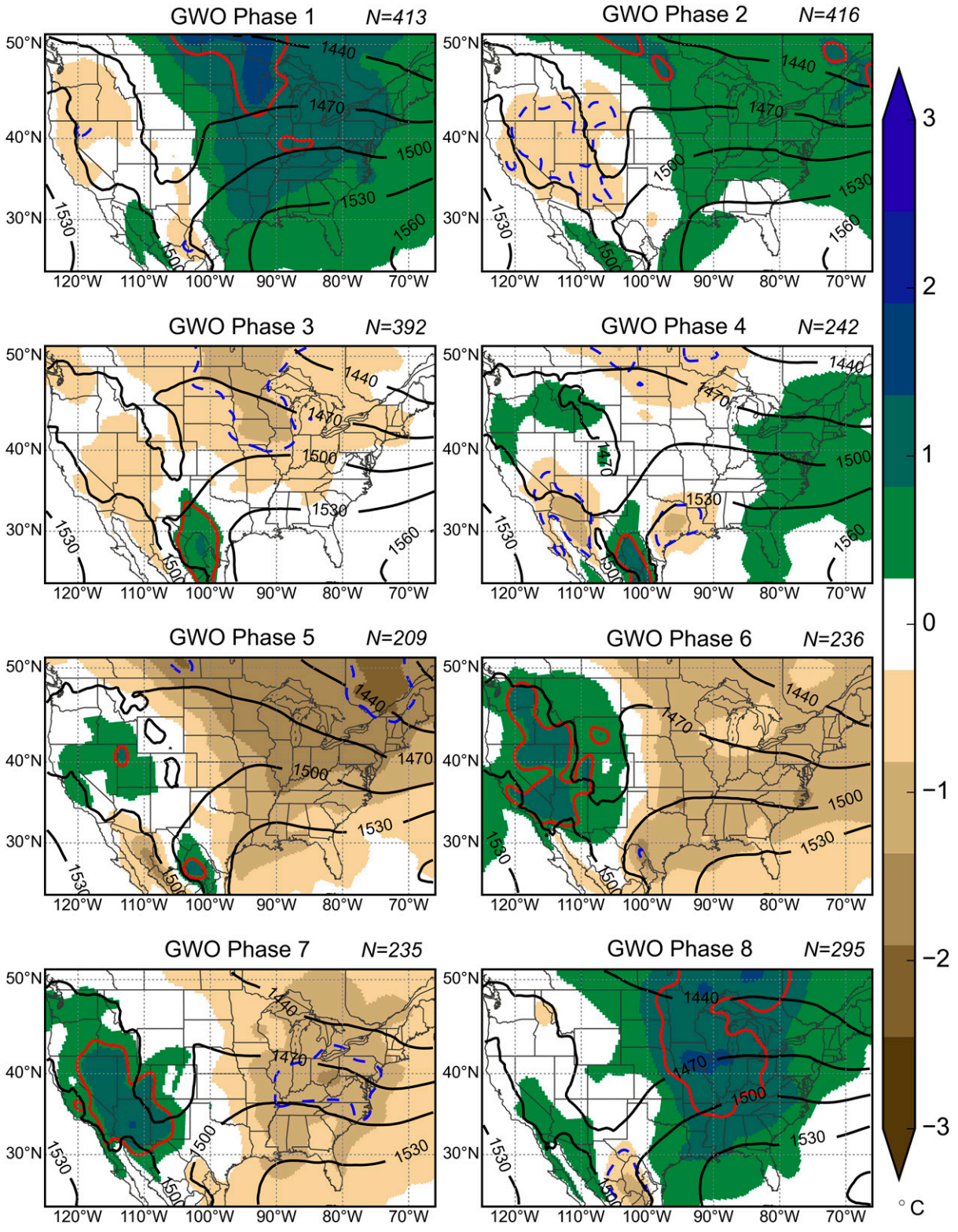

FIG. 3. GWO phase plots of average 850-hPa geopotential height (black contours) and surface dewpoint anomalies (color filled) relative to the March–June 1994–2013 climatology. Solid (dashed) red (blue) contours indicate statistical significance at the 95% confidence level. The *N* indicates the number of GWO phase days.

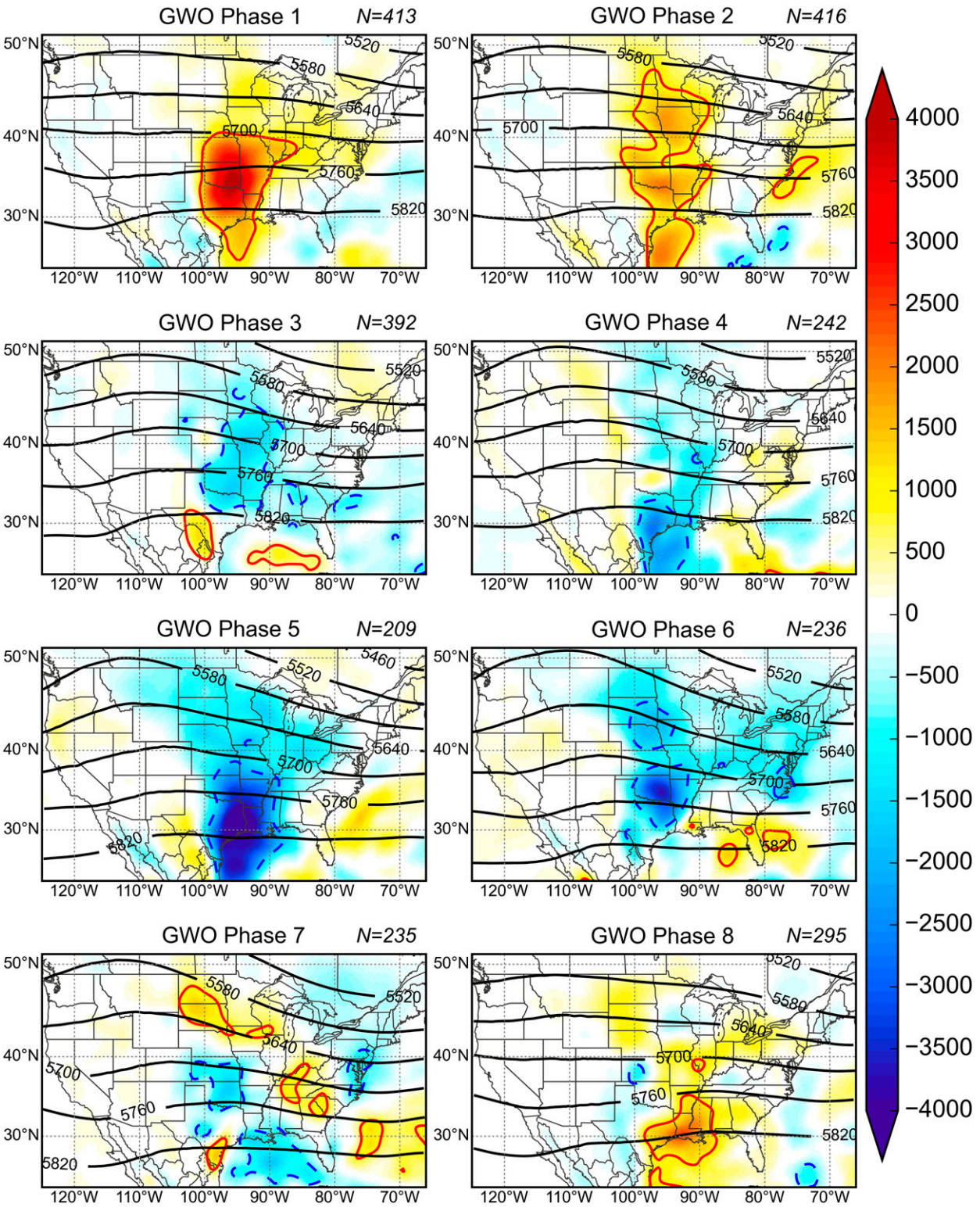

FIG. 4. As in Fig. 3, but for average 500-hPa geopotential height (black contours) and anomalies of the product of SBCAPE and BWD06.

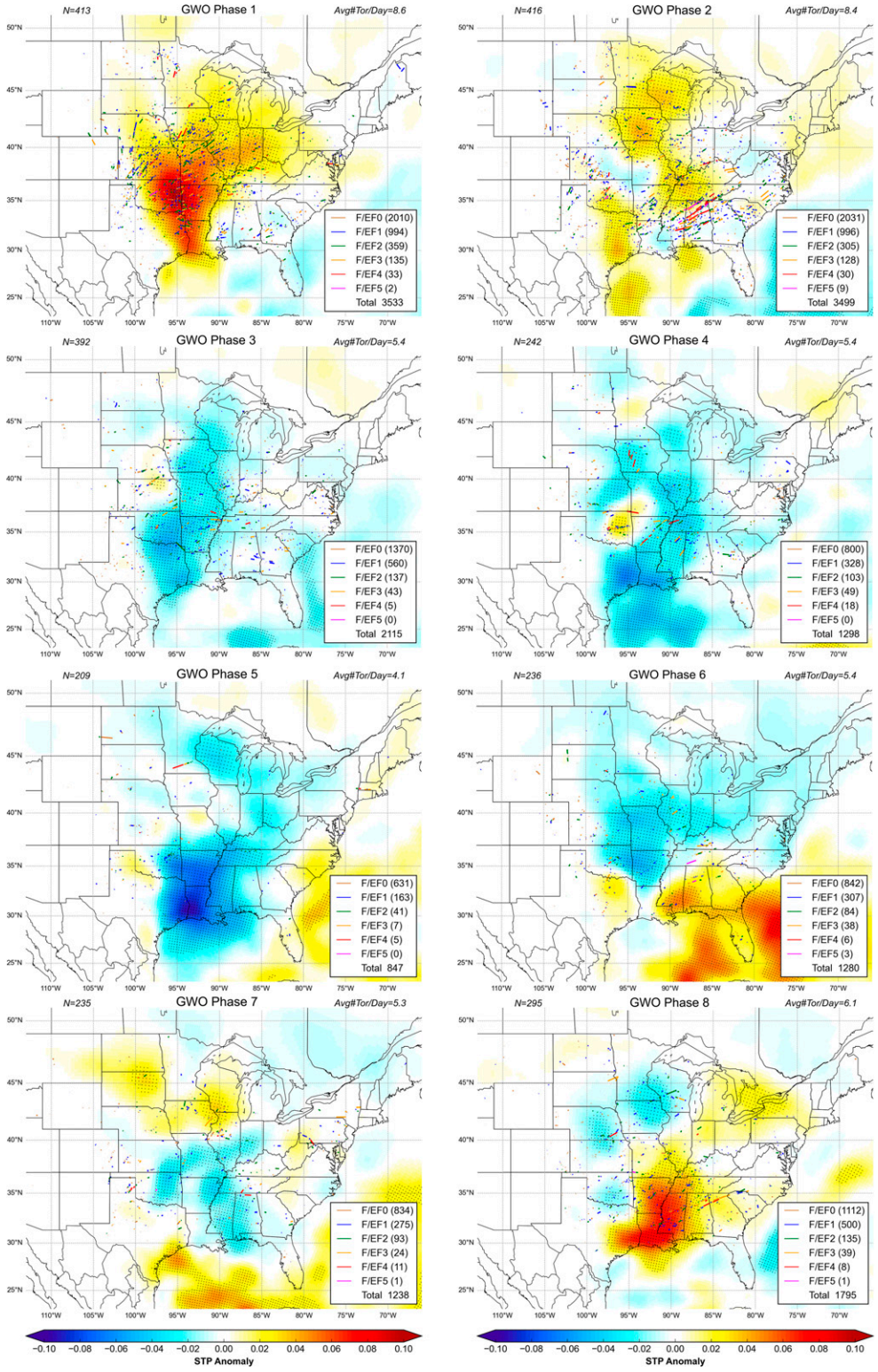

FIG. 5. March–June 1994–2013 STP anomalies (color filled) and tornado tracks by GWO phase. Statistical significance is stippled at the 95% confidence level. The *N* indicates the number of GWO phase days and ''Avg#Tor/Day'' indicates the average number of tornadoes reported per phase day.

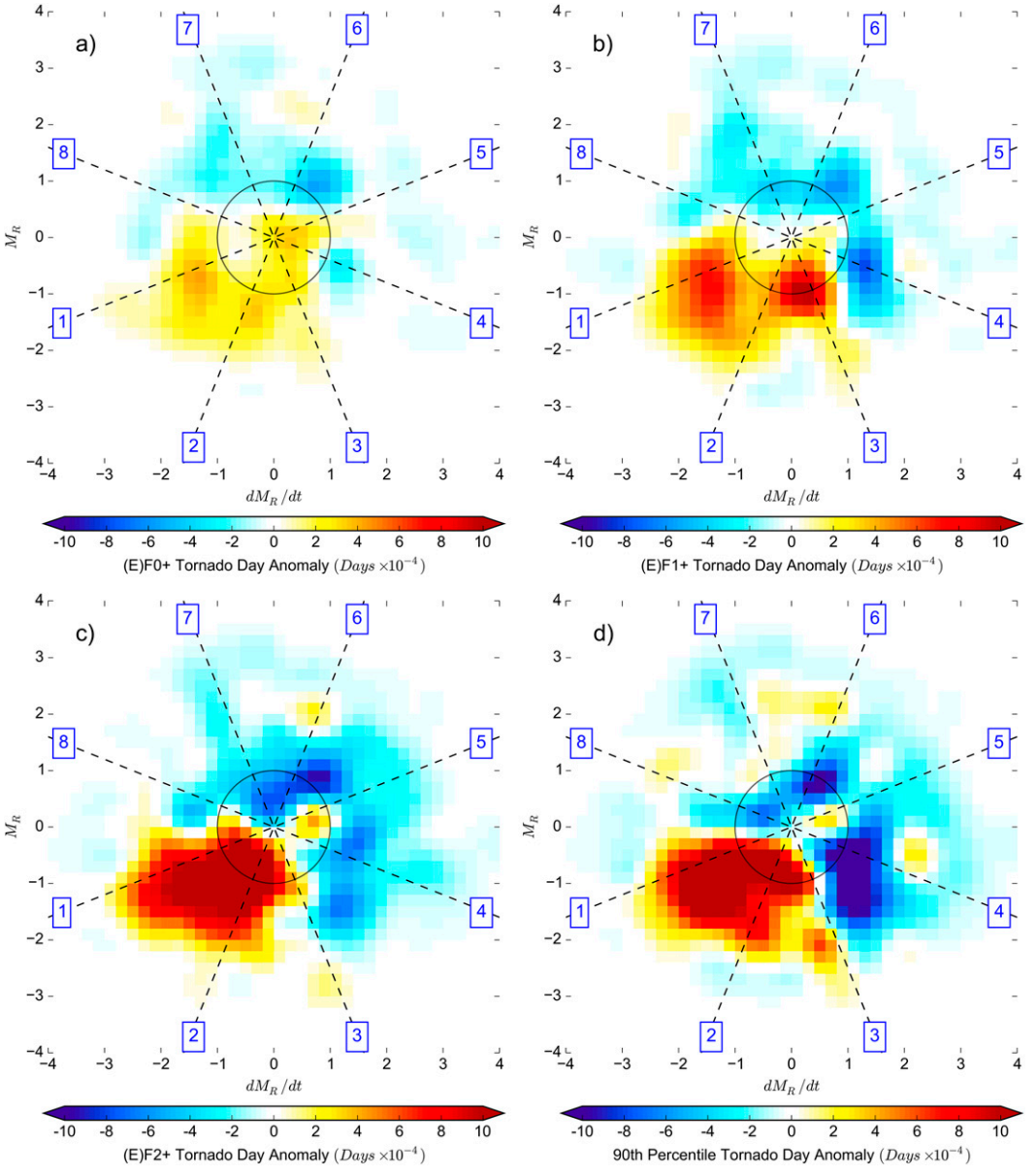

FIG. 6. GWO phase diagram of 1994–2013 binned anomalies of (a) (E)F0+ tornado days, (b) (E)F1+ tornado days, (c) (E)F2+ tornado days, and (d) 90th percentile tornado days ($N \sim 15$ tornadoes east of the Rocky Mountains) for the months March–June. The blue numbers in each plot indicate the GWO phase.

spring Intra-Americas low-level jet, which causes poleward surface water vapor flux into locations east of the Continental Divide (Muñoz and Enfield 2011). This regularly leads to positive equivalent potential temperature advection in places lee of the Rocky Mountains, providing necessary surface moisture and an unstable atmosphere essential for tornado-producing thunderstorms.

c. 90th percentile tornado days and tornado intensity

An important consideration in U.S. tornado frequency is the contribution from spatiotemporal event clustering, or so-called outbreak events. Tornado outbreaks, such as the devastating events of 27 April 2011 in the southeastern United States, cause the greatest socioeconomic loss and are of particular interest to researchers (Simmons and Sutter 2012). Here, we define these volatile days as a single day in which 15 or more tornadoes occur east of the Rocky Mountains. We recorded 285 tornado outbreak days out of a possible 2440 (~90th percentile). Plotting these ≥90th percentile tornado frequency days in GWO phase space, relative to the GWO climatology for March–June, yields noteworthy results (Fig. 6d). The 90th

percentile tornado frequency day exceedance is most likely to occur in anomalously low M_R and dM_R/dt phases (8, 1, and 2). Moreover, 90th percentile tornado frequency days are unlikely to occur during GWO phase 3. This result is significant, and could help describe recent patterns in the increasing trend of greater concentrations of tornadoes on fewer days (Brooks et al. 2014), although the relationship is not clear at this time. In addition to 90th percentile tornado days, phase space tornado day anomaly plots were created for (E)F0+ tornado days (Fig. 6a), (E)F1+ tornado days (Fig. 6b), and (E)F2+ tornado days (Fig. 6c). Again, the strongest signals for positive anomalies are found during anomalously low M_R and dM_R/dt phases.

4. Discussion and summary

The explanatory power of GWO during boreal spring in the United States is significant. Its use as a forecast tool for subseasonal tornado occurrence in the United States appears promising, but this study does not address such a question. Rather, the purpose here is to show the relationship wherein the frequency of tornado occurrence is significantly enhanced during periods when the time tendency of M_R is negative. Future work will investigate the potential utility of GWO as a tornado frequency predictor. However, a forecaster should note periods when the GWO becomes active and increases amplitude (phases 4, 5, and 6) via positive mountain and frictional torque, and increasing convection near the international date line (related to the MJO). This forces a stronger Hadley cell circulation, causing anomalous fluxes in the tropical meridional tropospheric wind component. As air is displaced poleward, it moves closer to the earth's axis of rotation, thus causing increases in the zonal wind component due to the conservation of angular momentum. An increase in Northern Hemisphere westerly momentum results, which produces an extension of the polar jet stream over the Pacific Ocean. This gives rise to positive M_R anomalies, characteristic of GWO phases 5 and 6. It is the decreasing tendency of M_R, and subsequent amplification of the polar jet stream over the Pacific Ocean (phases 8, 1, and 2) that favors synoptic weather patterns supportive of tornadoes east of the U.S. Rocky Mountains. These synoptic weather patterns include a midtropospheric trough in the western United States and a poleward flux in surface moisture across the Great Plains. A complete GWO circuit (counterclockwise orbit in phase space) can range from a broad range of 15–80 days (Weickmann and Berry 2009).

Monitoring and prediction of U.S. tornado frequency using the GWO will only be as skillful as the component calculations comprising M_R. Essentially, forecasting a GWO orbit will be contingent upon the predictability of the MJO and the engagement of the surface tourques that contribute to the global AAM budget. As our skill in predicting ENSO, MJO, and various other teleconnections increase, so too will our ability to capture all contributing components using the GWO framework. Thus, we recommend further analysis and prediction of the GWO if subseasonal forecasting of U.S. tornado occurrence is desired. We note, however, there will be no one magic index or parameter that will solve the complex interactions between components of our climate system in order to give extended lead time of tornado frequency. Instead, subseasonal forecasts for severe weather should understand that there are numerous physical processes involving multiple time and space scales that dictate where/when favorable conditions emerge for enhanced tornado frequency. This will ultimately allow forecasters to begin moving beyond the current one week limitation of U.S. tornado frequency prediction.

Acknowledgments. The authors thank Kimberly Hoogewind for providing routines to interpolate NARR data from pressure to AGL coordinates for calculation of STP fields and Dr. Charles Doswell III for reviewing an initial draft of the manuscript. Dr. David Gold, Ed Berry, and Klaus Weickmann provided critical feedback regarding GWO phase space and greatly improved the quality of this article. Finally, three anonymous reviewers and the editor provided valuable comments during the review process.

REFERENCES

Allen, J. T., M. K. Tippett, and A. H. Sobel, 2015: Influence of the El Niño/Southern Oscillation on tornado and hail frequency in the United States. *Nat. Geosci.*, **8**, 278–283, doi:10.1038/ngeo2385.

Anderson, J. R., and R. D. Rosen, 1983: The latitude-height structure of 40-50 day variations in atmospheric angular momentum. *J. Atmos. Sci.*, **40**, 1584–1591, doi:10.1175/1520-0469(1983)040<1584:TLHSOD>2.0.CO;2.

Barrett, B. S., and V. A. Gensini, 2013: Variability of central United States April–May tornado day likelihood by phase of the Madden–Julian Oscillation. *Geophys. Res. Lett.*, **40**, 2790–2795, doi:10.1002/grl.50522.

——, and B. N. Henley, 2015: Intraseasonal variability of hail in the contiguous United States: Relationship to the Madden–Julian oscillation. *Mon. Wea. Rev.*, **143**, 1086–1103, doi:10.1175/MWR-D-14-00257.1.

Brooks, H. E., J. W. Lee, and J. P. Craven, 2003: The spatial distribution of severe thunderstorm and tornado environments from global reanalysis data. *Atmos. Res.*, **67–68**, 73–94, doi:10.1016/S0169-8095(03)00045-0.

——, G. W. Carbin, and P. T. Marsh, 2014: Increased variability of tornado occurrence in the United States. *Science*, **346**, 349–352, doi:10.1126/science.1257460.

Brunet, G., and Coauthors, 2010: Collaboration of the weather and climate communities to advance subseasonal-to-seasonal prediction. *Bull. Amer. Meteor. Soc.*, **91**, 1397–1406, doi:10.1175/2010BAMS3013.1.

Cook, A. R., and J. Schaefer, 2008: The relation of El Niño–Southern Oscillation (ENSO) to winter tornado outbreaks. *Mon. Wea. Rev.*, **136**, 3121–3137, doi:10.1175/2007MWR2171.1.

Doswell, C. A., III, H. E. Brooks, and R. A. Maddox, 1996: Flash flood forecasting: An ingredients-based methodology. *Wea. Forecasting*, **11**, 560–581, doi:10.1175/1520-0434(1996)011<0560:FFFAIB>2.0.CO;2.

Gensini, V. A., and W. S. Ashley, 2011: Climatology of potentially severe convective environments from the North American regional reanalysis. *Electron. J. Severe Storms Meteor.*, **6** (8). [Available online at http://www.ejssm.org/ojs/index.php/ejssm/article/viewArticle/85.]

Grice, G., and Coauthors, 1999: The golden anniversary celebration of the first tornado forecast. *Bull. Amer. Meteor. Soc.*, **80**, 1341–1348, doi:10.1175/1520-0477(1999)080<1341:TGACOT>2.0.CO;2.

Hendon, H. H., 1995: Length of day changes associated with the Madden–Julian Oscillation. *J. Atmos. Sci.*, **52**, 2373–2383, doi:10.1175/1520-0469(1995)052<2373:LODCAW>2.0.CO;2.

Langley, R. B., R. W. King, I. I. Shapiro, R. D. Rosen, and D. A. Salstein, 1981: Atmospheric angular momentum and the length of day: A common fluctuation with a period near 50 days. *Nature*, **294**, 730–732, doi:10.1038/294730a0.

Lott, F., A. W. Robertson, and M. Ghil, 2001: Mountain torques and atmospheric oscillations. *Geophys. Res. Lett.*, **28**, 1207–1210, doi:10.1029/2000GL011829.

Madden, R. A., 1987: Relationships between changes in the length of day and the 40- to 50-day oscillation in the tropics. *J. Geophys. Res.*, **92**, 8391–8399, doi:10.1029/JD092iD07p08391.

——, and P. Speth, 1995: Estimates of atmospheric angular momentum, friction, and mountain torques during 1987–1988. *J. Atmos. Sci.*, **52**, 3681–3694, doi:10.1175/1520-0469(1995)052<3681:EOAAMF>2.0.CO;2.

Mesinger, F., and Coauthors, 2006: North American Regional Reanalysis. *Bull. Amer. Meteor. Soc.*, **87**, 343–360, doi:10.1175/BAMS-87-3-343.

Mo, K. C., and R. E. Livezey, 1986: Tropical-extratropical geopotential height teleconnections during the Northern Hemisphere winter. *Mon. Wea. Rev.*, **114**, 2488–2515, doi:10.1175/1520-0493(1986)114<2488:TEGHTD>2.0.CO;2.

Muñoz, E., and D. Enfield, 2011: The boreal spring variability of the Intra-Americas low-level jet and its relation with precipitation and tornadoes in the eastern United States. *Climate Dyn.*, **36**, 247–259, doi:10.1007/s00382-009-0688-3.

NOAA/NCDC, 2015: NCEP North American Regional Reanalysis (32km, 25 years). NOAA/NCDC, accessed 12 December 2015. [Available online at http://nomads.ncdc.noaa.gov/data.php#narr_datasets.]

NOAA/NWS Storm Prediction Center, 2015: Severe Weather Database Files (1950–2014). NOAA/NWS Storm Prediction Center, accessed 12 December 2015. [Available online at http://www.spc.noaa.gov/wcm/#data.]

Oort, A., 1997: Angular momentum cycle in planet earth. *Encyclopedia of Planetary Science*, J. H. Shirley and R. W. Fairbridge, Eds., Springer, 13–19.

Peixoto, J. P., and A. H. Oort, 1992: *Physics of Climate*. American Institute of Physics, 520 pp.

Simmons, K. M., and D. Sutter, 2012: The 2011 tornadoes and the future of tornado research. *Bull. Amer. Meteor. Soc.*, **93**, 959–961, doi:10.1175/BAMS-D-11-00126.1.

Thompson, D. B., and P. E. Roundy, 2013: The relationship between the Madden–Julian oscillation and U.S. violent tornado outbreaks in the spring. *Mon. Wea. Rev.*, **141**, 2087–2095, doi:10.1175/MWR-D-12-00173.1.

Thompson, R. L., R. Edwards, J. A. Hart, K. L. Elmore, and P. Markowski, 2003: Close proximity soundings within supercell environments obtained from the Rapid Update Cycle. *Wea. Forecasting*, **18**, 1243–1261, doi:10.1175/1520-0434(2003)018<1243:CPSWSE>2.0.CO;2.

Weickmann, K. M., 2003: Mountains, the global frictional torque, and the circulation over the Pacific–North American region. *Mon. Wea. Rev.*, **131**, 2608–2622, doi:10.1175/1520-0493(2003)131<2608:MTGFTA>2.0.CO;2.

——, and E. Berry, 2007: A synoptic-dynamic model of subseasonal atmospheric variability. *Mon. Wea. Rev.*, **135**, 449–474, doi:10.1175/MWR3293.1.

——, and ——, 2009: The tropical Madden–Julian oscillation and the global wind oscillation. *Mon. Wea. Rev.*, **137**, 1601–1614, doi:10.1175/2008MWR2686.1.

——, S. Khalsa, and J. Eischeid, 1992: The atmospheric angular-momentum cycle during the tropical Madden–Julian Oscillation. *Mon. Wea. Rev.*, **120**, 2252–2263, doi:10.1175/1520-0493(1992)120<2252:TAAMCD>2.0.CO;2.

——, G. N. Kiladis, and P. D. Sardeshmukh, 1997: The dynamics of intraseasonal atmospheric angular momentum oscillations. *J. Atmos. Sci.*, **54**, 1445–1461, doi:10.1175/1520-0469(1997)054<1445:TDOIAA>2.0.CO;2.

Wheeler, M. C., and H. H. Hendon, 2004: An all-season real-time multivariate MJO index: Development of an index for monitoring and prediction. *Mon. Wea. Rev.*, **132**, 1917–1932, doi:10.1175/1520-0493(2004)132<1917:AARMMI>2.0.CO;2.